

Low-Energy Antinucleon-Nucleus Interaction Revisited

E. Friedman

Received: date / Accepted: date

Abstract Annihilation cross sections of antiprotons and antineutrons on the proton between 50 and 400 MeV/c show Coulomb focusing below 200 MeV/c and almost no charge-dependence above 200 MeV/c. Similar comparisons for heavier targets are not possible for lack of overlap between nuclear targets studied with \bar{p} and \bar{n} beams. Interpolating between \bar{p} -nucleus annihilation cross sections with the help of an optical potential to compare with \bar{n} -nucleus annihilation cross sections reveal unexpected features of Coulomb interactions in the latter. Direct comparisons between \bar{n} -nucleus and \bar{p} -nucleus annihilations at very low energies could be possible if \bar{p} cross sections are measured on the same targets and at the same energies as the available cross sections for \bar{n} . Such measurements may be feasible in the foreseeable future.

Keywords Antinucleon-proton interaction · Antinucleon-nucleus interaction · Low energies

PACS 13.75.Cs · 24.10.Ht · 25.43.+t

1 Introduction

The motivation for the present work is the paper by Astrua et al. [1] reporting annihilation cross sections for antineutrons on six targets at momenta below 400 MeV/c. Very large cross sections were measured below 180 MeV/c but quantitative analyses have not been reported except noting that features of strong absorption are observed in these cross sections. Unfortunately direct comparisons with corresponding cross sections for antiproton-nucleus annihilation could not be made because experimental results are available mostly for

E. Friedman
Racah Institute of Physics, the Hebrew University, Jerusalem 91904, Israel
Tel.: +972-2-6584667
Fax: +972-2-6586347
E-mail: elifried@cc.huji.ac.il

Table 1 Experimental results for antinucleon-nucleus interaction at low energies

target	\bar{p} atoms	\bar{p} ann.	\bar{p} scatt.	\bar{n} ann.
C	+		+	+
O	+			
Ne		+		
Al				+
Ca	+		+	
Fe	+			
Ni	+	+		
Cu				+
Zr	+			
Ag				+
Cd	+			
Sn	+	+		+
Te	+			
Pt		+		
Pb	+		+	+
data points	90	7	88	42

different targets at different energies. In contrast, annihilation cross sections for antiprotons and antineutrons on the proton are available between 50 and 400 MeV/c, showing the expected Coulomb effects at the lower end of this range and hardly any dependence on charge at the higher end.

Table 1 shows a schematic summary of available experimental results for low energy antinucleon interactions with nuclei. It is seen that only for Sn there are results for both \bar{p} and \bar{n} annihilation cross sections, (but not at the same energies). In order to compare between \bar{n} and \bar{p} annihilation cross sections on nuclear targets, we use optical-model interpolations for \bar{p} . The present work includes some updates compared to Ref. [2] where more details are included.

In Sect. 2 we compare total annihilation cross sections for $\bar{p}p$ and $\bar{n}p$ at very low energies and describe the mechanism of Coulomb focusing which is very responsible for the large differences observed. In Sect. 3 we establish an optical-model approach to the \bar{p} -nucleus interaction which is used in Sect. 4 for comparisons with the results of Ref. [1] for \bar{n} -nucleus cross sections. In the summary (Sect. 5) it is proposed to match the existing data of annihilation cross sections for \bar{n} on nuclei by measuring annihilation cross sections for \bar{p} on the same targets at the corresponding energies, in an attempt to shed light on what appears to be a puzzle.

2 Antiproton and antineutron annihilation on the proton

Figure 1 shows experimental annihilation cross sections of \bar{p} and \bar{n} on the proton. All the \bar{n} cross sections and the \bar{p} cross sections below 180 MeV/c, open circles and solid circles, respectively, were measured by the OBELIX collaboration [3,4,5,6] and the \bar{p} cross sections above 180 MeV/c, solid triangles, were measured by Brückner et al. [7] using a different experimental setup. The

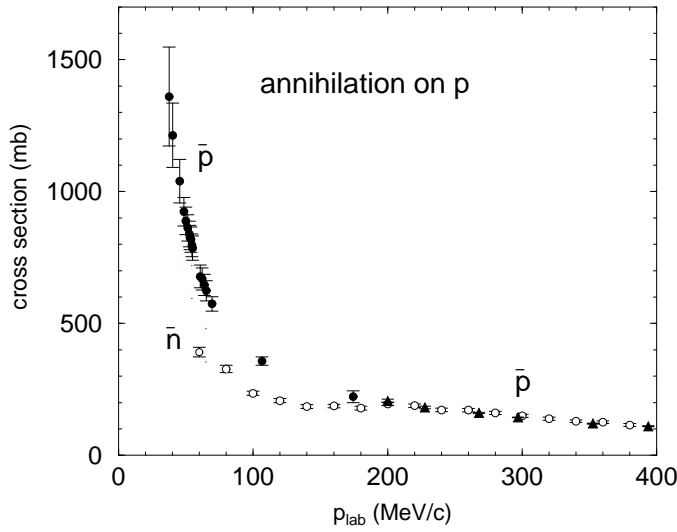


Fig. 1 Experimental annihilation cross sections for \bar{p} and \bar{n} on the proton, see text for references. Open circles for \bar{n} , filled circles and triangles for \bar{p} .

figure shows that the results in the two momentum ranges join very smoothly and that above 200 MeV/c there are no observed differences between the $\bar{p}p$ and $\bar{n}p$ cross sections, although the former contains contributions of I=0 and I=1 isospin states whereas the latter is a pure I=1 isospin state.

The \bar{n} cross sections increase as the energy goes down, most likely due to the expected $1/v$ dependence of the s -wave cross section. However, the increase of the cross sections for the \bar{p} is much stronger than the increase for \bar{n} , resulting from the Coulomb focusing effect which has been observed in annihilation cross sections of \bar{p} on nuclei [8]. For very strong absorption which is typical of antiproton interactions, the ‘black disk’ cross section πR^2 , with R the radius, is replaced, classically, by πd_0^2 where d_0 is the impact parameter for which the distance of closest approach is R . A straight-forward calculation yields for the total reaction cross section

$$\sigma_R = \pi R^2 \left(1 + \frac{m + M}{M} \frac{Ze^2}{RE_{lab}} \right) \quad (1)$$

with m and M the masses of the \bar{p} and target nucleus, respectively, and E_{lab} the lab. kinetic energy. A quantum-mechanical calculation [8] leads to an identical result for the Coulomb enhancement factor

$$\sigma_R = \pi R^2 \left(1 + \frac{2mZe^2}{\hbar^2 k_{lab} k R} \right) \quad (2)$$

with k and k_{lab} the cm and lab wave numbers, respectively. It was shown in [8] that at very low energies $\sigma_R \approx ZR \approx ZA^{1/3}$, and for $R = 1.84 + 1.12A^{1/3}$ fm good agreement with experiment is obtained.

Table 2 Energies and momenta where the Coulomb enhancement factor is 2

target	R(fm)	E_{lab} (MeV)	p_{lab} (MeV/c)
p	3.0	1.0	43
C	4.4	2.1	63
Cu	6.3	6.6	112
Sn	7.4	9.8	136
Pb	8.5	14	162

Table 2 shows calculated energies and momenta where the Coulomb enhancement factor is 2. For a proton target that momentum is near 45 MeV/c, as is indeed observed in Fig. 1. It is therefore concluded that at very low energies the major differences between \bar{p} and \bar{n} annihilation on the proton are due to the Coulomb focusing effect.

3 Antiproton-nucleus optical potential

Having demonstrated that the differences between low energy \bar{p} and \bar{n} annihilation cross sections on the proton are fully explained by the Coulomb focusing effect, we turn to the \bar{n} annihilation cross sections on six nuclear targets between C and Pb [1]. Here it is impossible to compare directly between experimental results and we use an optical potential to calculate cross sections for \bar{p} on the same targets and at the same energies as for the \bar{n} measurements. Only an outline is presented here as more details are given in [2].

For very low energies of interest we begin by analyzing the extended and precise experimental results for strong interaction effects in antiprotonic atoms, adopting the ‘global’ analysis of 90 data points across the periodic table done a decade ago [9]. The simplest ‘ $t\rho$ ’ form of the optical potential is

$$2\mu V_{opt}(r) = -4\pi \left(1 + \frac{\mu}{m} \frac{A-1}{A}\right) [b_0(\rho_n + \rho_p) + b_1(\rho_n - \rho_p)] \quad , \quad (3)$$

where μ is the reduced mass of the \bar{p} , ρ_n and ρ_p are the neutron and proton density distributions normalized to the number of neutrons N and number of protons Z , respectively, $A = N + Z$, and m is the mass of the nucleon. The complex parameters b_0 and b_1 are determined by fits to the data. The isovector coefficient b_1 was shown in [9] to be consistent with zero and as we found in the previous section that no isovector dependence is observed in the annihilation cross sections on the proton, we set $b_1=0$ for the rest of this work. Finite range folding of a \bar{p} -nucleon interaction is also included [9].

Proton densities were obtained from experimentally determined charge densities of nuclei. Neutron densities were approximated by two-parameter Fermi distributions, characterized by the difference between rms radii of neutron density and the corresponding proton density distribution in nuclei, parameterized by [10]

$$r_n - r_p = \gamma \frac{N - Z}{A} + \delta. \quad (4)$$

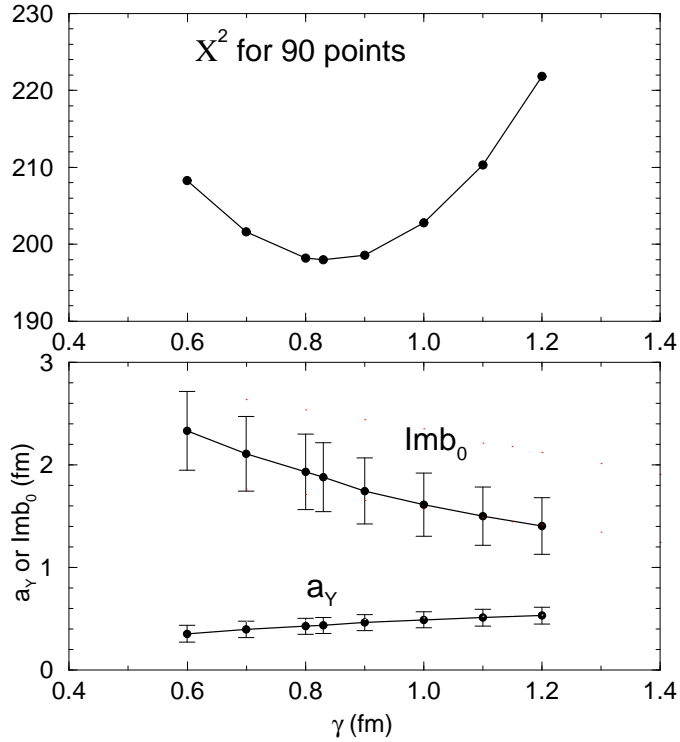


Fig. 2 Summary of global fits to \bar{p} atoms as function of the neutron density parameter γ of Eq.(4) using a Yukawa-type \bar{p} -nucleon interaction. Top: χ^2 values for 90 data points, bottom: resulting parameters $\text{Im } b_0$ and a_Y , see text.

Figure 2 shows examples of fits to the data for a Yukawa-type \bar{p} -N interaction. The minimum in χ^2 is obtained for a value of the parameter γ which implies values of $r_n - r_p$ in agreement with the great majority of results regarding these differences, obtained by a variety of methods [11,12,13]. In [2] similar results are presented for a Gaussian interaction. It is worth noting that the rms radii involved and the strong interaction parameters b are the same, within errors, for the two interaction models.

The above optical potential was shown in [2] to reproduce very well angular distributions for elastic scattering of \bar{p} by C, Ca and Pb at 300 MeV/c. We therefore proceed to calculate from this potential annihilation cross sections for \bar{p} on the same targets as used in the \bar{n} experiment [1].

4 Antineutron-nucleus annihilation cross sections

The optical potential derived above for \bar{p} -nucleus interaction was used to calculate annihilation cross section for \bar{p} and \bar{n} on the six targets at the seven energies studied by Astrua et al. [1]. Applying the \bar{p} potential also to calculate

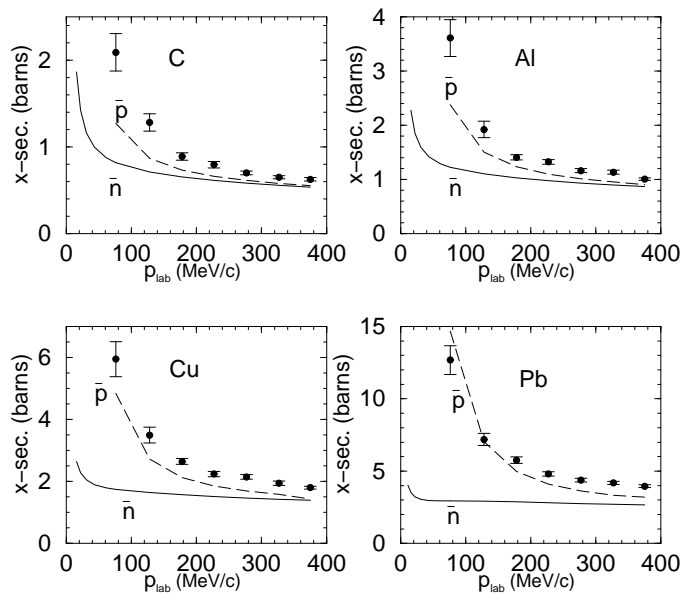


Fig. 3 Comparing calculation with experiment for total annihilation cross sections on nuclei using the potential derived in Sect. 3. Solid curves for \bar{n} , dashed curves for \bar{p} . Experimental results for \bar{n} are from [1]. See also [2].

annihilation cross sections of \bar{n} is justified in this energy range because no trace of isovector-dependence was observed neither in the antinucleon annihilation on the proton (Sect. 2) nor in the optical potential for antiprotonic atoms [9]. Moreover, total $\bar{p}p$ cross sections do not show any sign of structure up to 420 MeV/c [14].

Figure 3 compares calculated cross sections for \bar{p} and \bar{n} with experimental annihilation cross sections for \bar{n} on nuclei. The start of the $1/v$ rise for \bar{n} at the lower momenta is seen, shifting to lower and lower momenta as the size of the nucleus increases. The calculated \bar{p} cross sections increase sharply at low momenta compared to the *calculated* cross sections for \bar{n} , as expected. In fact, the momenta where the ratio of the calculated \bar{p} to \bar{n} cross sections is 2 are in remarkable agreement with table 2, showing the dominance of Coulomb focusing at low momenta. Surprisingly, the experimental cross sections for the \bar{n} cross sections follow closely the corresponding calculated cross sections for antiprotons. In particular, the sharp rise of the experimental cross sections for antineutrons at low momenta follows remarkably well the calculated cross sections for antiprotons. This is in sharp contrast with the experimental results for a proton target, as is seen in Fig. 1.

A direct comparison between experimental cross sections on nuclei is possible only for a Sn target where a preliminary result is available for \bar{p} at 100 MeV/c [15]. Figure 4 shows the single measured \bar{p} cross section and the seven experimental \bar{n} cross sections in relation to the calculated annihilation

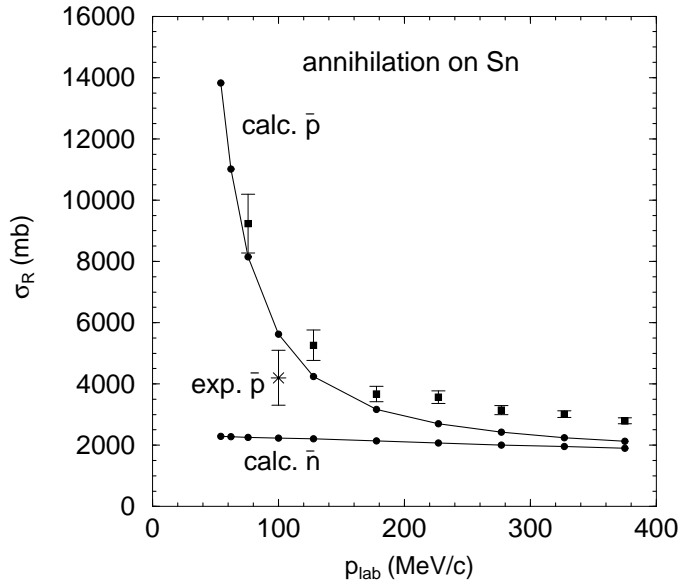


Fig. 4 Comparing calculation with experiment for total annihilation cross sections on Sn using the potential derived in Sect. 3. Experimental results for \bar{n} (circles) are from [1] and a single experimental result for \bar{p} (star) is from [15]. This supersedes a similar figure in [2].

cross sections from the present optical potential. The figure suggests that measured \bar{n} cross sections around 100 MeV/c are larger than the corresponding \bar{p} cross sections, which is at variance with the results for a proton target as seen in Fig. 1. Coulomb focusing (table 2) suggests that the \bar{n} annihilation cross sections on Sn are expected to be a factor of 3 *smaller* than the corresponding \bar{p} cross sections near 100 MeV/c.

5 Summary

Total annihilation cross sections for antiprotons and antineutron on the proton show smooth variation with energy between lab momenta of 50 and 400 MeV/c. The marked increase of the \bar{p} cross sections relative to the \bar{n} ones below 200 MeV/c is fully consistent with the effect of Coulomb focusing. Above that momentum the cross sections for the two types of projectile are practically identical, suggesting that annihilation cross sections at low energies are insensitive to isospin effects. Phenomenological optical potentials reproduce well all the available results for \bar{p} -nucleus interaction from antiprotonic atoms to elastic scattering and annihilation cross section up to 600 MeV/c, with no evidence for an isovector term. Consequently this potential is used to calculate annihilation cross sections, and comparisons with the measured \bar{n} -nucleus cross section reveal unexpected features of Coulomb effects. No explanation for this result is known at present.

Direct comparison between experimental cross sections without the help of a model is currently possible only for a single measurement on Sn (in addition to the many results for a proton target) and that shows the \bar{n} cross section to be larger than the \bar{p} one. An experimental approach to this ‘puzzle’ may be possible in the foreseeable future by measuring total annihilation cross sections for antiprotons on the six nuclear targets of Astrua et al. [1] and at the same energies.

Acknowledgements I wish to thank T. Bressani for useful discussions and for providing in numerical form the detailed results of Ref. [6]. Discussions with A. Gal and A. Levitan are gratefully acknowledged.

References

1. Astrua M., et al.: Antineutron-nucleus annihilation cross sections below 400 MeV/c, Nucl. Phys. A 697, 209-224 (2002)
2. Friedman E.: Antineutron and antiproton interaction at very low energies, Nucl. Phys. A 925, 141-149 (2014)
3. Bertin A., et al.: $\bar{p}p$ annihilation cross section at very low energy, Phys. Lett. B 369, 77-85 (1996)
4. Zenoni A., et al.: New measurements of the $\bar{p}p$ annihilation cross section at very low energy, Phys. Lett. B 461, 405-412 (1999)
5. Benedettini A., et al.: $\bar{p}p$ partial cross sections at low energy, Nucl. Phys. B (Proc. Suppl.) 56A, 58-65 (1997)
6. Bertin A., et al.: Study of $\bar{n}p$ annihilation in two mesons in the momentum range between 50 to 400 MeV/c with OBELIX, Phys. Lett. B 410, 344-352 (1997)
7. Brückner W., et al.: Measurements of the antiproton-proton annihilation cross section in the beam momentum range between 180 and 600 MeV/c, Z. Phys. A 335, 217-229 (1990)
8. Batty C.J., Friedman E., Gal A.: Unified optical-model approach to low-energy antiproton annihilation on nuclei and to antiprotonic atoms, Nucl. Phys. A 689, 721-740 (2001)
9. Friedman E., Gal A., Mareš J.: Antiproton-nucleus potentials from global fits to antiprotonic X-rays and radiochemical data, Nucl. Phys. A 761, 283-295 (2005)
10. Friedman E., Gal A.: In-medium interactions of Low-energy hadrons, Phys. Reports 452, 89-153 (2007)
11. Jastrzębski J., et al.: Neutron density distributions from antiprotonic atoms compared with hadron scattering data, Int. J. Mod. Phys. E 13, 343-351 (2004)
12. Friedman E.: Unified approach to nuclear densities from exotic atoms, Hyperfine Interact. 193, 33-38 (2009)
13. Tarbert C.M., et al.: The neutron skin of ^{208}Pb from coherent pion photoproduction, Phys. Rev. Lett. 112, 242502 (2014)
14. Bugg D.V., et al.: $\bar{p}p$ total cross sections below 420 MeV/c, Phys. Lett. B 194, 563-567 (1987)
15. Bianconi A., et al.: Measurement of the antiproton-nucleus annihilation cross section at 5.3 MeV, Phys. Lett. B 704, 461-466 (2011).